



# High-temperature glassy-ceramic sealants $\text{SiO}_2\text{--Al}_2\text{O}_3\text{--BaO--MgO}$ and $\text{SiO}_2\text{--Al}_2\text{O}_3\text{--ZrO}_2\text{--CaO--Na}_2\text{O}$ for solid oxide electrochemical devices

S. QI<sup>1</sup>, N. M. POROTNIKOVA<sup>2,3</sup>, M. V. ANANYEV<sup>2,3</sup>, A. V. KUZMIN<sup>2,3</sup>, V. A. EREMIN<sup>2,3</sup>, A. A. PANKRATOV<sup>2</sup>, N. G. MOLCHANOVA<sup>2</sup>, O. G. REZNITSKIKH<sup>2</sup>, A. S. FARLENKOV<sup>2,3</sup>, E. G. VOVKOTRUB<sup>2</sup>, Yu. P. ZAIKOV<sup>2,3</sup>

1. College of Material Sciences and Engineering, Beijing University of Chemical Technology, Beijing 100029, China;

2. Institute of High-Temperature Electrochemistry of UB RAS, Ekaterinburg 620137, Russia;

3. Ural Federal University named after the First President of Russia B. N. Yeltsin, Ekaterinburg 620002, Russia

Received 12 November 2015; accepted 25 May 2016

**Abstract:** Glasses of the  $\text{SiO}_2\text{--Al}_2\text{O}_3\text{--BaO--MgO}$  and  $\text{SiO}_2\text{--Al}_2\text{O}_3\text{--ZrO}_2\text{--CaO--Na}_2\text{O}$  systems were synthesized in the perspective to apply them as sealants in SOFC at operating temperatures of 700–900 °C. Thermal properties of the chosen glass compositions and their compatibility with the SOFC materials (YSZ-electrolyte and alloy-interconnector Crofer22APU, 15X25T) were investigated by means of synchronic thermal analysis and high-temperature dilatometry. The elemental analysis was performed by atomic emission spectroscopy. The average values of the temperature coefficients of the linear extension are  $10.0 \times 10^{-6} \text{ }^\circ\text{C}^{-1}$  for glass 45% $\text{SiO}_2\text{--}15\%\text{Al}_2\text{O}_3\text{--}25\%\text{BaO--}15\%\text{MgO}$  and  $9.5 \times 10^{-6} \text{ }^\circ\text{C}^{-1}$  for glass 60% $\text{SiO}_2\text{--}10\%\text{Al}_2\text{O}_3\text{--}10\%\text{ZrO}_2\text{--}5\%\text{CaO--}15\%\text{Na}_2\text{O}$ . The gluing microstructure in YSZ/glass/Crofer22APU was studied by scanning electron microscopy. The crystallization process of silicate phases was revealed to occur in the  $\text{SiO}_2\text{--Al}_2\text{O}_3\text{--BaO--MgO}$  glass. The analysis of the crystallization products was performed by Raman spectroscopy and X-ray diffraction. Glassy ceramics was proved to possess better parameters in comparison with amorphous glass to be used as a sealant in electrochemical sensors and oxygen sensors. The  $\text{SiO}_2\text{--Al}_2\text{O}_3\text{--ZrO}_2\text{--CaO--Na}_2\text{O}$  low-temperature amorphous glass can be applied in SOFC.

**Key words:** glassy-ceramic sealants; SOFC; YSZ; Crofer22APU; magnesium silicate

## 1 Introduction

A variety of materials used in electrochemical devices, such as SOFC, electrolyzers, and electrochemical gas sensors generate a need for a constant search of novel sealants. At present, high-temperature silicate glasses are well proved as materials for sealing cells of electrochemical devices (ECD) [1]. It is revealed in a series of works that glassy sealants are very good sealers, which can operate in fuel cells over 1000 h without any significant degradation of their properties [2–4].

Nowadays, yttrium doped zirconium dioxide is used as a SOFC electrolyte. It has significant oxygen ion conductivity at high temperatures of 800–900 °C. The SOFC anode and cathode are made of nickel-cermet (Ni-YSZ) and strontium-manganite (LSM), respectively. Researchers have recently attempted to decrease the SOFC operation temperature to 700–800 °C, which

would greatly widen the list of possible construction materials and would increase its working life. There are some requirements for sealants, such as chemical stability both in reduction and in oxidation ambient, lack of interaction with functional materials for ECD, low conductance, good adhesion and mechanic durability, close coefficients of thermal expansion with the functional materials, good viscosity at cell operating temperatures. The advantage of using glassy-sealants in electrochemical devices is that it is possible to optimize the glass chemical composition by varying chemical composition and an oxide concentration in the composition. Thus, the mechanical durability, resistance, and coefficient of thermal expansion (CTE) can be changed. It stands to mention that it is vital to choose a sealant composition for each particular construction, considering chemical compatibility requirements and CTEs, to glue different parts of the high temperature electrochemical device whether it is ceramics/ceramics or ceramics/metal. The CTEs of SOFC components are

generally  $9.5 \times 10^{-6}$ – $12 \times 10^{-6}$  K<sup>-1</sup> for the electrolyte (YSZ, GDC, LSGM),  $12 \times 10^{-6}$ – $14 \times 10^{-6}$  K<sup>-1</sup> for the cathode,  $10 \times 10^{-6}$ – $14 \times 10^{-6}$  K<sup>-1</sup> for the anode, and  $11 \times 10^{-6}$ – $15 \times 10^{-6}$  K<sup>-1</sup> for the interconnect [1,5–7].

The special ceramic glues, which are obtained on the basis of different oxides, boratic acid, glasses, are used to obtain a solid high-temperature joint of ceramics. Thus, in a number of works [8], the compositions of ceramic glues for gluing and sealing were patented. The gluing temperature of the suggested compositions reaches 1400 °C.

There are two basic types of glassy-sealants, which currently are being studied and used in the SOFC: amorphous high-temperature glass and glass-ceramics. The glass sealants perfectly serve as sealant materials at high temperatures (600–900 °C). They become viscous, and as a result, it is possible to reduce a tension between SOFC functional parts, and to vary a cell design and performance [9–12]. However, during long exploitation life glass sealants can devitrify, i.e., their crystallization takes place. Thus, they become less viscous at high temperatures, while thermocycling can lead to fragility and decrepitation of the material [13–16]. The glass sealants also interact with interconnectors made of heat-resistant alloys, which leads to the iron and chromium leaching. This involves an additional increase in rate of devitrification and, consequently, a decrease in chemical stability of the sealant [17].

The amorphous high-temperature glass is capable of sustaining an insignificant tension and cracks in SOFC. At appropriate SOFC operation, while thermocycling, this type of glass performs not only as gluing material for functional parts, but also as viscous sealant, serving in situ. Hence, it allows sealing leakages during long operation, which, otherwise, can destroy all the flow. This type of glass cannot crystallize during all term of the sealant exploitation, otherwise its mechanical and hermetical properties sharply decay [18,19]. The amorphous high-temperature glass is heated to the temperature close to the melting point (which also can coincide with the SOFC operating temperature). As a result, small cracks formed during thermocycling can be healed due to the amorphous nature of the glass. This glass sealant is good for short-term use [20]; however, eventually the self-recovering glass has a tendency to crystallization. It results in a loss of self-recover function and makes the glass-sealant vulnerable to tensions and cracking, causing cell leakage [20–22].

The glassy-ceramic sealants are initially crystallized glasses, which have a very solid physical structure [21]. This glass can be of interest, because it is stronger than most of the other types of glasses and does not change in time at constant coefficient of thermal expansion [23].

There are a large number of works dedicated to

studying the glassy sealants based on silicate glasses [24–32]. For example, BaO–CaO–Al<sub>2</sub>O<sub>3</sub>–B<sub>2</sub>O<sub>3</sub>–SiO<sub>2</sub> (BCAS) glass-ceramics have been investigated as sealants for testing the large size planar anode supported SOFCs [24]. The CTE of the BCAS glass with heat treatment for different times matched that of YSZ and Crofer22APU. Needle-like barium silicate, barium calcium silicate and hexacelsian can be found in the glass after heat-treatment at 750 °C for 50 h. The open circuit voltage (OCV) of the cell kept 1.19 V at 750 °C. No cracks or pores were found in the interface between the glass-ceramics and component.

HEYDARI et al [25] reported the development of suitable glass-ceramic sealants based on the CaO–BaO–B<sub>2</sub>O<sub>3</sub>–Al<sub>2</sub>O<sub>3</sub>–SiO<sub>2</sub> system to be used in anode-supported SOFC stacks at 700 °C, and their mechanical properties and sinterability of this system were also studied. Mechanical properties of this glass were improved with increasing heat-treatment time because barium silicate, barium calcium silicate and hexacelsian phases crystallized.

The effects of zirconium oxide on the crystallization, densification and dielectric properties of the CaO–MgO–Al<sub>2</sub>O<sub>3</sub>–SiO<sub>2</sub> glass were investigated in Refs. [26,27]. The glass transition temperature and onset crystallization temperature increased with rising zirconia content. The phyllosiloxide and anorthite crystallites were observed in sequence during sintering at 800–950 °C for pure CaO–MgO–Al<sub>2</sub>O<sub>3</sub>–SiO<sub>2</sub> glass. The phyllosiloxide phase crystallized mainly via surface nucleation, which inhibited further viscous flow densification. The crystallization temperature of phyllosiloxide shifted from 800 to 850 °C after adding ZrO<sub>2</sub>. For the sample with 8% (mass fraction) ZrO<sub>2</sub> sintered at 850 °C, homogeneously distributed tetragonal zirconia precipitates accompanied a small amount of acicular phyllosiloxide in the glass matrix. As well in Ref. [28], it was found that the addition of zirconia nanoparticles up to 10% (volume fraction) improved mechanical properties without causing any negative effect on thermal and electrical properties.

It was demonstrated [29] that adding and increasing the amount of BaO in the examined glass-ceramic materials from the SiO<sub>2</sub>–Al<sub>2</sub>O<sub>3</sub>–Na<sub>2</sub>O–K<sub>2</sub>O–CaO system caused significant changes in the phase composition as well as an increase in the content of crystalline phases. The addition of BaO to the SiO<sub>2</sub>–Al<sub>2</sub>O<sub>3</sub>–Na<sub>2</sub>O–K<sub>2</sub>O–MgO samples caused considerable changes with regard to the phase composition and an increase in the crystalline phase content [30].

The effect of iron oxide on the sealants properties was studied in Refs. [31,32]. In Ref. [31] the crystallization peak temperature decreased, the crystallization activation energy increased, and the

crystal granularity decreased with the addition of  $\text{Fe}_2\text{O}_3$  to the  $\text{CaO-Al}_2\text{O}_3\text{-SiO}_2$  system. The ESR results indicate that  $\text{Fe}_2\text{O}_3$  can adjust the network structure of the glass-ceramics, allowing  $\text{Fe}^{3+}$  to assume an octahedral coordination, which enhances the bending strength of the glass-ceramics. In Ref. [32] the endothermic peak temperature of about 760 °C associated with the transition and the exothermic peak temperature of about 1000 °C associated with crystallization were found when the  $\text{Fe}_2\text{O}_3\text{-CaO-MgO-Al}_2\text{O}_3\text{-SiO}_2$  basic glass was heated. The  $\text{Fe}_2\text{O}_3$  content increase results in the glass transition temperature and crystallization temperature decrease.

In the present study, the systematic investigations related to amorphous glass and glassy-ceramics in the  $\text{SiO}_2\text{-Al}_2\text{O}_3\text{-BaO-MgO}$  and  $\text{SiO}_2\text{-Al}_2\text{O}_3\text{-ZrO}_2\text{-CaO-Na}_2\text{O}$  systems, which are good sealants for the electrochemical devices, were carried out.

## 2 Experimental

### 2.1 Synthesis and attestation

The sealant materials in two systems of  $\text{SiO}_2\text{-Al}_2\text{O}_3\text{-BaO-MgO}$  and  $\text{SiO}_2\text{-Al}_2\text{O}_3\text{-ZrO}_2\text{-CaO-Na}_2\text{O}$  were synthesized. Based on the thermal analysis data, two optimal compositions: 45% $\text{SiO}_2$ -15% $\text{Al}_2\text{O}_3$ -25% $\text{BaO}$ -15% $\text{MgO}$  and 60% $\text{SiO}_2$ -10% $\text{Al}_2\text{O}_3$ -10% $\text{ZrO}_2$ -5% $\text{CaO}$ -15% $\text{Na}_2\text{O}$  were chosen for testing as sealants in electrochemical devices.

The chemical composition of the  $\text{SiO}_2\text{-Al}_2\text{O}_3\text{-BaO-MgO}$  high-temperature glass was specified by mixing talc, barium and aluminum oxide. The talc composition was  $\text{Mg}_3\text{Si}_4\text{O}_{10}(\text{OH})_2$  with admixtures of 1.2%  $\text{Al}_2\text{O}_3$ , 0.5%  $\text{CaO}$  and 1.4%  $\text{Fe}_2\text{O}_3$ . The barium oxide was taken as  $\text{BaCO}_3$  (high purity), and  $\text{Al}_2\text{O}_3$  was of a reagent grade. The initial components for low-temperature synthesis of glass with the composition of  $\text{SiO}_2\text{-Al}_2\text{O}_3\text{-ZrO}_2\text{-CaO-Na}_2\text{O}$  were  $\text{SiO}_2$  (reagent grade),  $\text{ZrO}_2$  (high purity),  $\text{Al}_2\text{O}_3$  (reagent grade),  $\text{CaCO}_3$  (high purity), and  $\text{Na}_2\text{CO}_3$  (high purity).

The batch components mixture in a required mass ratio was ground with isopropyl alcohol and dried at 120 °C. The preliminarily synthesis was carried out in a porcelain cup during 3 h at 1100 and 900 °C for high- and low-temperature glass, respectively. At the next stage, the annealed batch was separated into pieces and melted in a crucible made of stabilized zirconium oxide at 1400 °C. The crucible for glass melting had a special design: in the lower part of the crucible there was an opening with a diameter of 4 mm, into which a sleeve was inserted. While reaching certain temperature the molten glass dripped through the sleeve into reservoir with distilled water. This method allowed not to exceed the necessary temperature, and hence, to avoid

evaporation of volatile components.

The obtained glass was ground into a fine powder in the porcelain mortar in order to use it for elementary analysis and to glue ceramic materials and alloy-interconnectors. The samples for measuring the coefficient of thermal expansion were pressed and annealed at 1100 and 850 °C for high- and low-temperature glass, respectively.

The elemental analysis was performed by atomic emission spectroscopy with inductively coupled plasma at the spectrometer Optima 4300 DV (Perkin Elmer, USA). The summary error of determination did not exceed 2%–3%.

X-ray powder diffraction was carried out using the Rigaku conventional diffractometer D/MAX-2200V (Rigaku, Japan) in radiation  $\text{Cu K}_\alpha$  ( $\lambda=0.15418$  nm) in the angle interval of  $10^\circ < 2\theta < 90^\circ$  at the angle scanning rate of 0.3 (°)/s.

### 2.2 Thermal properties

The gluing temperature was determined according to the shape. The gluing temperature was considered as the temperature, at which a smooth transparent drop of glass of spherical shape was formed.

The DSC measurements were carried out by the thermal analysis device STA 449 F1 Jupiter (NETZSCH, Germany). The glass sample as a powder with a mass of 3 g was placed into a platinum crucible and heated with the rate of 0.6 °C/s in the temperature range of 35–1200 °C. The measuring cell together with the sample was aerated with the rate of  $3.3 \times 10^{-7} \text{ m}^3/\text{s}$ . The dependences at heating and cooling of the measurement cell were recorded; the heating rate was 10 °C/min.

The thermal extension of glasses and SOFC functional materials was investigated using the quartz dilatometer using an automatic installation with digital measuring set “Tesatronic TT-80” (gage probe TESA GT 21HP, scale range  $\pm 200 \mu\text{m}$ , delicacy 0.01  $\mu\text{m}$ ) on samples with the length of  $\sim 15$  mm. The measurements were performed in air with the heating rate of 0.33 °C/s in the range of 30–900 °C. A specimen in a shape of ruby monocrystallic rod was used as the etalon for the dilatometer. A discrepancy with tabular data for the coefficient of thermal expansion did not exceed 4%, at that, the mean-square error for experimental dependence which characterized a spread of points was 0.01%–0.05%.

### 2.3 Microstructure

Microstructure characterization and measurement of the element composition of gluing for the YSZ/glass/Crofer22APU were carried out by scanning electron microscope (SEM) JSM 5900LV with microanalyzer INCA Energy 200 (JEOL Oxford, Japan)

and MIRA 3LMU (TESCAN, Czech Republic). The YSZ/glass/Crofer22APU sample used to study the gluing microstructure has a “sandwich” structure. It is composed of two  $1\text{ cm} \times 1.5\text{ cm} \times 0.1\text{ cm}$  plates (electrolyte and steel), which are connected by a glassy sealant. To prepare the sample a suspension of a ground glass in ethyl hydroxide was used. The gluing temperature corresponds to the temperature of glass softening  $1100$  and  $900^\circ\text{C}$  with a  $10\text{ min}$  dwelling for high- and low-temperature glass, respectively. The samples were pretreated by the epoxy impregnation technique under vacuum in order to take SEM images and then cross-sections of the samples were obtained with the use of diamond suspension at the polishing-grinding machine Struers Labopol.

The Raman spectroscopy was used to study the crystalline phase of the high-temperature glass of  $\text{SiO}_2\text{--Al}_2\text{O}_3\text{--BaO--MgO}$  composition. Measurements were conducted by the Raman microscope-spectrometer U 1000 (Renishaw, England). This spectrometer allowed recording Raman spectra of samples with a space resolution up to  $1\text{ }\mu\text{m}$ . The cross-section of the YSZ/glass/Crofer22APU was tested. The tests were performed in the range from  $50$  to  $1200\text{ cm}^{-1}$ , and with time exposition of  $30\text{ s}$ . The operating conditions were as follows: capacity of the He/Ne laser ( $633\text{ nm}$ ) was  $1\text{ mW}$ , spectral resolution was  $2\text{ cm}^{-1}$ , accuracy of wave number was  $\pm 1\text{ cm}^{-1}$ , size of laser spot was  $1\text{ }\mu\text{m}$  at room temperature in air atmosphere. The Si line ( $99.9999\%$ )  $520\text{ cm}^{-1}$  was used as an etalon.

### 3 Results and discussion

Tests were carried out with glasses, which exhibited the best results at gluing the ceramic samples of zirconium–yttrium electrolyte:  $45\%\text{SiO}_2\text{--}15\%\text{Al}_2\text{O}_3\text{--}25\%\text{BaO--}15\%\text{MgO}$  is the high-temperature glass No. 1,  $60\%\text{SiO}_2\text{--}10\%\text{Al}_2\text{O}_3\text{--}10\%\text{ZrO}_2\text{--}5\%\text{CaO--}15\%\text{Na}_2\text{O}$  is the low-temperature glass No. 2. The glasses compositions are listed in Table 1.

**Table 1** Chemical composition of investigated glasses

Sample No.	Composition/%						
	$\text{SiO}_2$	$\text{Al}_2\text{O}_3$	$\text{BaO}$	$\text{CaO}$	$\text{MgO}$	$\text{ZrO}_2$	$\text{Na}_2\text{O}$
1	44.7	14.9	25.1	–	15.3	–	–
2	59.6	11.0	–	3.4	–	10.6	15.4

The gluing temperatures for samples No. 1 and No. 2 compositions were  $(1240 \pm 10)$  and  $(950 \pm 10)^\circ\text{C}$ , respectively. At indicated temperatures the smooth transparent drops of spherical shape, free of impurities inclusions, were formed from the glass powders.

The thermal analysis data at heating and cooling are

shown in Fig. 1. Two exothermic peaks are observed at  $882$  and  $951^\circ\text{C}$  on the DSC curve for the high-temperature glass, that allows assuming the existence of at least two crystallizing processes proceeding up to the glass melting temperature. Possibly, the manganese silicates of different chemical compositions crystallized out. It is important to note that there are no crystallization peaks on the cooling curve that can testify irreversibility of this process when heating.

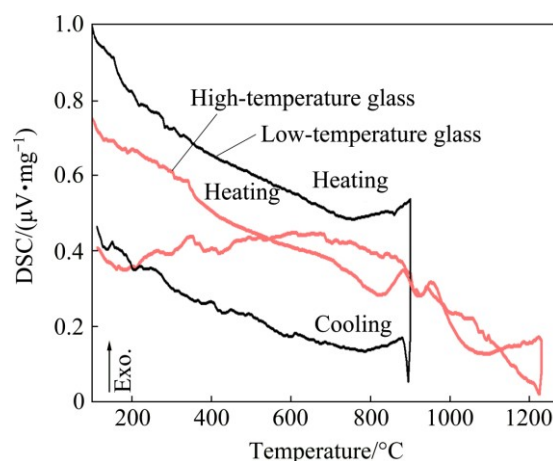


**Fig. 1** DSC dependences for investigated silicate glasses samples

The softening temperatures of the glasses under analysis are hard to detect using the DSC dependences. A small slope was revealed in the region of  $600\text{--}700^\circ\text{C}$  for a low temperature glass and in the region of  $680\text{--}745^\circ\text{C}$  for a high temperature glass, which denotes a glass transition temperature.

The temperature dependences of the linear extension for glasses, YSZ ceramics and Crofer22APU, 15X25T alloy-interconnectors are shown in Fig. 2. On the extension dependences the smooth sections, close to the linear function, can be indicated within the temperature range of  $50\text{--}600^\circ\text{C}$ . At further heating there

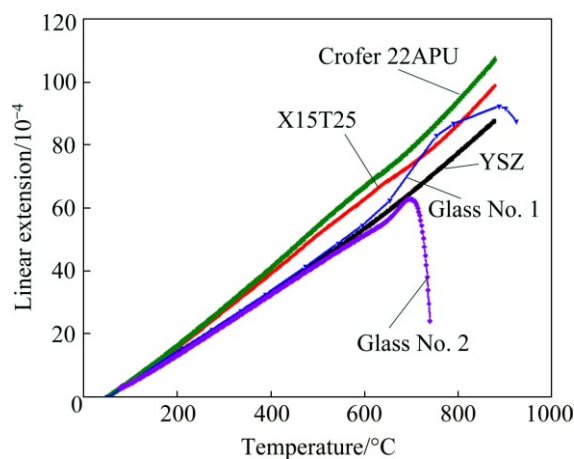


**Fig. 2** Temperature dependences for linear extension of silicate glasses and functional materials of SOFC

is a softening of glasses at 850 and 700 °C for glasses No. 1 and 2, respectively. The dilatometric curves of both glasses defined the glass transition temperature ( $T_g$ ) and softening temperature ( $T_s$ ). The results are presented in Table 2. The difference between  $T_s$  and  $T_g$  was observed for high temperature glass, which involves a parallel process of high temperature glass crystallization.

**Table 2** Thermal properties of different specimens

Sample No.	Coefficient of thermal extension ( $10^{-6} \text{ }^{\circ}\text{C}^{-1}$ )	Glass transition temperature ( $T_g$ )/ $^{\circ}\text{C}$	Softening temperature ( $T_s$ )/ $^{\circ}\text{C}$
1	10.0	670	890
2	9.5	650	700

The average values of the thermal extension coefficient, calculated in the range of 50–600 °C, were  $10.0 \times 10^{-6} \text{ }^{\circ}\text{C}^{-1}$  for the high-temperature glass (Sample No. 1) and  $9.5 \times 10^{-6} \text{ }^{\circ}\text{C}^{-1}$  for the low-temperature glass (Sample No. 2).

These values are in acceptable agreement with the thermal extension coefficient of Crofer22APU alloy ( $12.3 \times 10^{-6} \text{ }^{\circ}\text{C}^{-1}$ ) and alloy 15X25T ( $11.8 \times 10^{-6} \text{ }^{\circ}\text{C}^{-1}$ ) in the indicated range. However, it is vital to prevent thermal and pressure expansions to eliminate cracking and delamination of the sealant.

The XRD patterns for the investigated glasses are presented in Fig. 3. The obtained data clearly specify its amorphous structure with broadened peak at  $25^{\circ}$ – $30^{\circ}$ . XRD patterns of the glasses heat-treated at 800, 900 and 1000 °C at a heating rate of 30 °C/min, which were soaked at these temperatures for 15 min, are shown in Fig. 4.

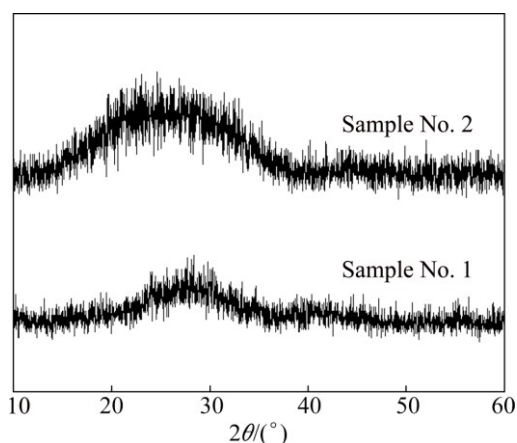


**Fig. 3** XRD patterns of investigated silicate glasses

The cross-section SEM images of the YSZ/glass/Crofer22APU interface were taken in order to investigate the microstructure of the silicate glasses. Figure 5 shows SEM images of gluing in the mode of back-scattering electrons (BSE), allowing recording the phase contrast due to the different average atomic number.

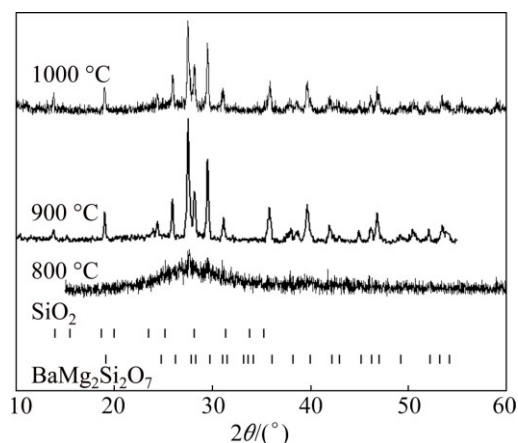


**Fig. 4** XRD patterns for high-temperature glass sample No. 1 at various temperatures

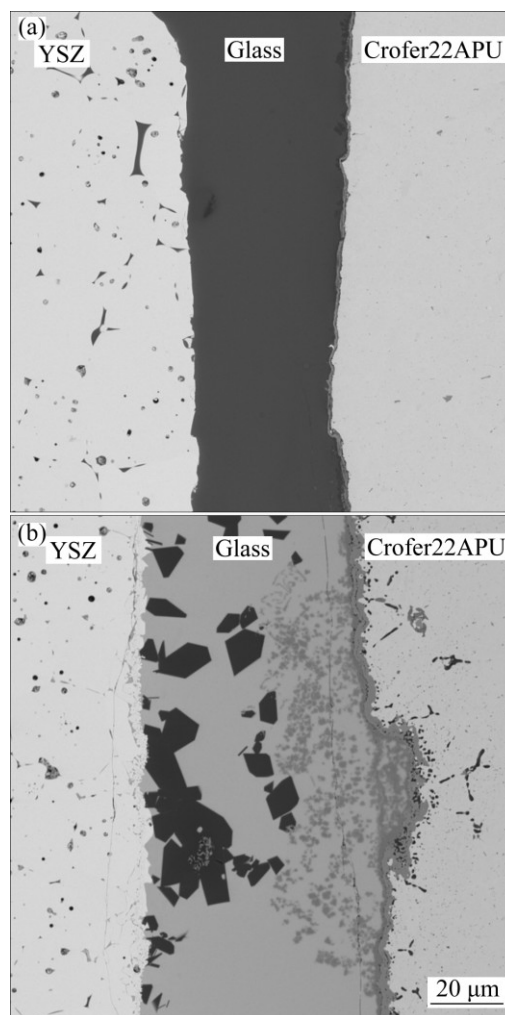


**Fig. 5** Cross-section SEM images of YSZ/glass/Crofer22APU interface: (a) Sample No. 2; (b) Sample No. 1

According to the SEM image of YSZ/ $\text{SiO}_2$ - $\text{Al}_2\text{O}_3$ - $\text{ZrO}_2$ - $\text{CaO}$ - $\text{Na}_2\text{O}$ /Crofer22APU illustrated in Fig. 5(a) the interaction products of glass with steel are not formed. This fact allows recommending the low-temperature amorphous glass for usage as a sealant in SOFC.



It is seen in the SEM images that the investigated silicate glasses possess a good adhesion to the YSZ materials and Crofer22APU alloy as well as low porosity, and lack of significant gluing defects. Hence, these glasses can be applied as sealants. For the high-temperature glass No. 1 the phases of crystallization (dark crystals) can be seen, which are localized close to the electrolyte interphase; besides, there is morphologically more light and fine phase along the glass/Crofer 22APU interface.

The energy-dispersion analysis was carried out with the purpose of the elementary qualitative and quantitative analysis of the surface that helps to understand the chemical composition of formed phases. According to the analysis (Fig. 6), it was proved that the dark crystalline phases of glass consist of Mg, Si and O elements in a ratio of approximately 2:1:3.5. Possibly, the manganese silicate phases with different chemical compositions ( $\text{Mg}_2\text{SiO}_4$ ,  $\text{MgSiO}_3$  etc.) are formed, and a layer at the interface with the Crofer22APU alloy is a chrome oxide layer. Chrome oxide, apparently, is formed at gluing functional parts when contacting with air up to the temperature of glass softening.

The Raman spectra were obtained at different sectors in order to specify the phase composition of

formed crystalline phases in high-temperature glass No. 1 (Fig. 7). It is clear that at different sectors the specific peaks differ from each other. The authors of papers [33–36] reported that generally the Raman spectra can be divided into four areas: below 400, 550–800, 800–1300, and 1300–1600  $\text{cm}^{-1}$ . The peaks up to 400  $\text{cm}^{-1}$  are related to the deformation vibrations of Si—O—M; the deformation vibration of Si—O—Si is within 550–800  $\text{cm}^{-1}$ ; the vibration mode of the wave number in the range from 800 to 1300  $\text{cm}^{-1}$ , according to works [37,38], is connected with the valent vibrations of Si—O in tetrahedral  $[\text{SiO}_4]$ . In Refs. [39,40] the specific lines for manganese silicate are presented. In the spectral range of 500–700  $\text{cm}^{-1}$  the authors pointed out lines typical for  $\text{MgSiO}_3$  with the perovskite structure, which correlate with our data in Figs. 7(c) and (b), whereas in the range from 800 to 1000  $\text{cm}^{-1}$  there are specific lines for  $\text{MgSiO}_3$  with the ilmenite structure,  $\beta\text{-Mg}_2\text{SiO}_4$  and  $\gamma\text{-Mg}_2\text{SiO}_4$  (Figs. 7(a) and (b)).

The typical Raman spectra for YSZ and Crofer22APU alloy are shown in Fig. 8. The Raman spectra for the alloy (Fig. 8(c)) are essentially featureless, because metals and alloys have a simple chemical composition and high symmetry and do not have characteristic peaks.

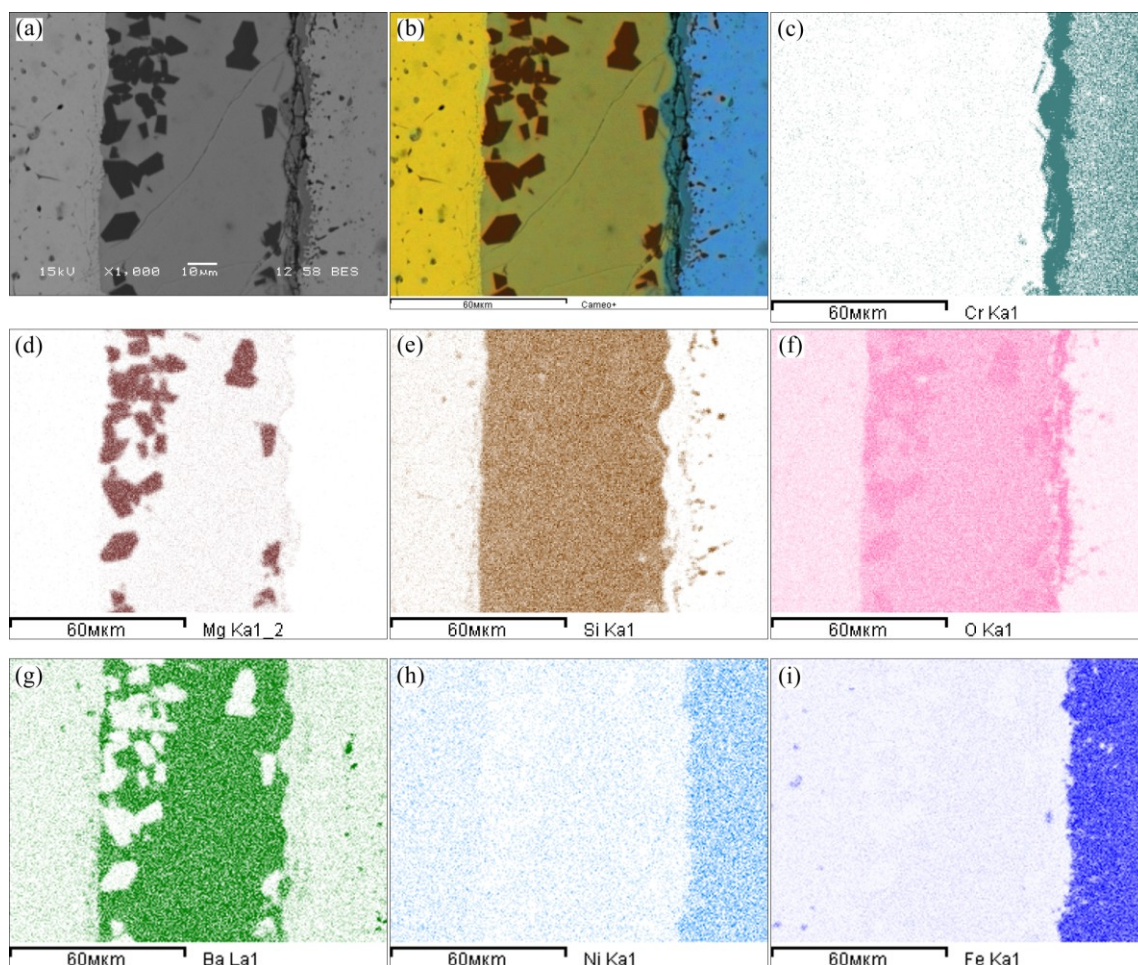
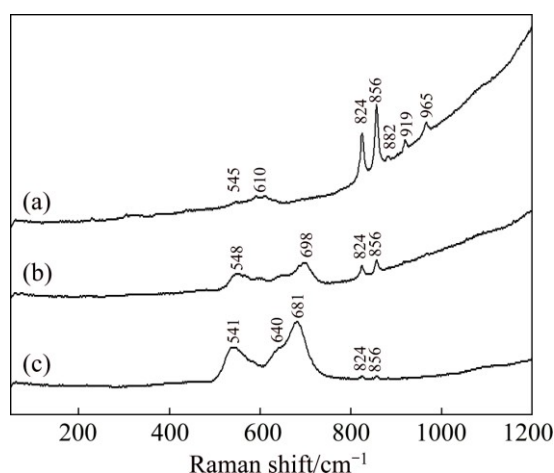
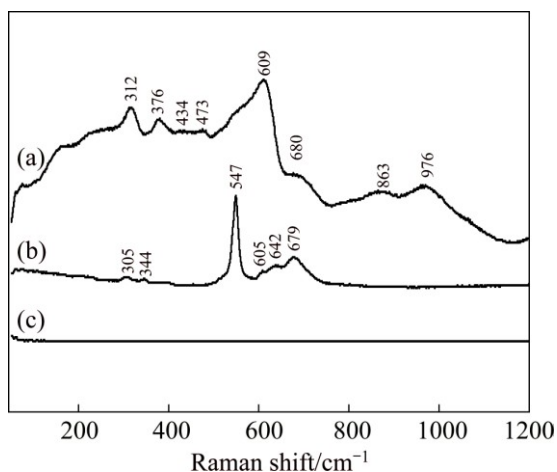


Fig. 6 EDX mapping of YSZ/glass No. 1/Crofer22APU interface



**Fig. 7** Raman spectra for high-temperature glass No. 1 at different sectors of gluing: (a) b-Mg<sub>2</sub>SiO<sub>4</sub>; (b) g-Mg<sub>2</sub>SiO<sub>4</sub>+MgSiO<sub>3</sub>; (c) MgSiO<sub>3</sub>



**Fig. 8** Raman spectra for YSZ (a), Cr<sub>2</sub>O<sub>3</sub> (b) and Crofer 22APU alloy (c)

The obtained type of spectra for the YSZ electrolyte is in a good agreement with the literature data [41]. The Raman spectrum for the YSZ area (Fig. 8(a)) has one intensive line at  $\sim 609\text{ cm}^{-1}$  and several weak lines. An appearance of numerous lines for the YSZ phase indicates that the YSZ surface does not have ideal cubic structure, and the electrolyte suffers the tetragonal and monoclinous deformations [42–45].

The Raman spectrum of chromium oxide with intensive peak at  $547\text{ cm}^{-1}$  and several weak peaks at 305, 344, 605, 642, 679  $\text{cm}^{-1}$  are shown in Fig. 8(b). The obtained data is in a good agreement with the results of work [46], where for the Cr<sub>2</sub>O<sub>3</sub> oxide the specific peaks correspond to  $554\text{ cm}^{-1}$  and are about  $620\text{ cm}^{-1}$ , and for the CrO<sub>2</sub> oxide a wide assymmetric line with maximum at  $660\text{ cm}^{-1}$  is the typical one.

The glasses studied in this work were tested for gluing planar and tubular fragments of the YSZ solid

electrolytes while manufacturing the trial samples for electrochemical devices: solid oxide sensors, oxygen pumps, and solid oxide fuel cells (Fig. 9). The oxygen pump manufactured using the composite glass No. 1, continuously exploits at 800–900 °C, stands over 200 heat/cooling cycles and, at that, saves full leaktightness of construction. This was determined by the lack of gaseous oxygen leakage through the external construction space into internal one.



**Fig. 9** Picture of oxygen pump made with composite glass No. 1

## 4 Conclusions

The glasses of 45%SiO<sub>2</sub>–15%Al<sub>2</sub>O<sub>3</sub>–25%BaO–15%MgO (No. 1), 60%SiO<sub>2</sub>–10%Al<sub>2</sub>O<sub>3</sub>–10%ZrO<sub>2</sub>–5%CaO–15%Na<sub>2</sub>O (No. 2) compositions, perspective as sealants for YSZ and alloys-interconnectors, were obtained.

It was demonstrated that the average values of temperature coefficients of the linear extension, calculated in the range of 50–600 °C, are  $10.0 \times 10^{-6}\text{ }^{\circ}\text{C}^{-1}$  for glass No. 1 and  $9.5 \times 10^{-6}\text{ }^{\circ}\text{C}^{-1}$  for glass No. 2. They are in a good agreement with the coefficient of thermal expansion of solid YSZ electrolyte and a little lower than that of the alloys-interconnectors.

Two exothermic peaks at 882 and 951 °C are observed at the DSC curve, which allows assuming that two crystallization processes occur up to the glass melting temperature.

The energy-dispersed analysis specified that the glass crystalline phases consist of Mg, Si, and O elements, and likely, the manganese silicate phases are formed. The layer at the interphase with Crofer22APU alloy is the chrome oxide film. The obtained Raman spectra proved our suggestions concerning the phase composition of formed crystalline phases in high-temperature glass No. 1.

The glass with the SiO<sub>2</sub>–Al<sub>2</sub>O<sub>3</sub>–BaO–MgO composition containing crystalline phases, revealed to be the most perspective for usage as sealants in high-temperature electrochemical devices, such as electrochemical sensors and oxygen sensors.

The SiO<sub>2</sub>–Al<sub>2</sub>O<sub>3</sub>–ZrO<sub>2</sub>–CaO–Na<sub>2</sub>O low-temperature amorphous glass can be applied in SOFC, because this

composition is stable against Cr-containing steels.

## Acknowledgments

This work was partly supported by the program “Fundamental research program for the development of the Arctic zone of the Russian Federation”, the Russian Foundation for Basic Research, project No. 14-29-04009; supported by Act 211 of Government of the Russian Federation, agreement No. 02.A03.21.0006 and Russian President scholarship 2015-2017 CII-1572.2015.1 and CII-1663.2015.1. The research was partially performed using the facilities of the Shared Access Centre “Composition of Compounds”.

This work is done by the co-worker of Research and Advanced Development in the framework of the project “Development and creation of high-technological manufactory of autonomic multipurpose power sources based of domestic high-technological solid oxide fuel cells” (No. 02.G25.31.0198 by 27.04.2016) under financial support of the Ministry of Education and Science of Russian Federation in accordance with Government of Russian Federation Decree by 09.04.2010 N 218.

## References

- [1] FERGUS J W. Sealants for solid oxide fuel cells [J]. *Journal of Power Sources*, 2005, 147: 46–57.
- [2] CHOU Y S, STEVENSON J W, CHOI J P. Evaluation of a single of cell and candidate materials with high water content hydrogen in a genetic solid oxide fuel cell stack test fixture, Part II: Materials and interface characterization [J]. *International Journal of Applied Ceramic Technology*, 2013, 10(1): 97–106.
- [3] DONALD I W, MALLINSON P M, METCALFE B L, GERRARD L A, FERNIE J A. Recent developments in the preparation, characterization and applications of glass- and glass-ceramic-to-metal seals and coating [J]. *Journal of Materials Science*, 2011, 46: 1975–2000.
- [4] REDDY A A, TULYAGANOV D U, PASCUAL M J, KHARTON V V, TSIPIS E V, KOLOTYGIN V A, FERREIRA J M F. Diopside-Ba disilicate glass-ceramic sealants for SOFCs: Enhanced adhesion and thermal stability by Sr for Ca substitution [J]. *International Journal of Hydrogen Energy*, 2013, 38: 3073–3086.
- [5] SINGHAL S C, KENDALL K. High temperature solid oxide fuel cells: Fundamentals, design and applications [M] Amsterdam: Elsevier, 2003.
- [6] OSINKIN D A, BRONIN D I, BERESNEV S M, BOGDANOVICH N M, ZHURAVLEV V D, VDOVIN G K, DEMYANENKO T A. High-performance anode-supported solid oxide fuel cell with impregnated electrodes [J]. *Journal of Solid State Electrochemistry*, 2014, 18: 149–156.
- [7] OSINKIN D A, BOGDANOVICH N M, BERESNEV S M, ZHURAVLEV V D. High-performance anode-supported solid oxide fuel cell with impregnated electrodes [J]. *Journal of Power Sources*, 2015, 288: 20–25.
- [8] BRUSENCOV V P. Solid oxide fuel cells: Collection of scientific and technical articles [M] Snezhinsk: Publisher RFNC-VNIIEF, 2003.
- [9] LESSING P A. A review of sealing technologies applicable to solid oxide electrolysis cells [J]. *Journal of Materials Science*, 2007, 42(10): 3465–3476.
- [10] MAHAPATRA M K, LU K. Glass-based seals for solid oxide fuel and electrolyzer cells — A review [J]. *Materials Science and Engineering R*, 2010, 67: 65–85.
- [11] BASU R N, BLASS G, BUCHKREMER H P, STOVER D, TIETZ F, WESSEL E, VINKE I C. Simplified processing of anode-supported thin film planar solid oxide fuel cells [J]. *Journal of the European Ceramic Society*, 2005, 25: 463–471.
- [12] BASU R N, SHARMA A D, DUTTA A, MUKHOPADHYAY J. Processing of high performance anode supported planar solid oxide fuel cells [J]. *International Journal of Hydrogen Energy*, 2008, 33: 5748–5754.
- [13] LEY K L, KRUMPELT M, KUMAR R, MEISER J H, BLOOM I. Glass ceramic sealants for SOFCs. Part I: Physical properties [J]. *Journal of Materials Research*, 1996, 11: 1489–1493.
- [14] EICHLER K, SOLOW G, OTSCHIK P, SCHAFFRATH W. BAS glasses for high temperature applications [J]. *Journal of the European Ceramic Society*, 1999, 19: 1101–1104.
- [15] SOHN S B, CHOI S Y. Suitable glass ceramic sealants for planar solid oxide fuel cells [J]. *Journal of the American Ceramic Society*, 2004, 87: 254–260.
- [16] LARSEN P H, JAMES P F. Chemical stability of MgO–CaO–Cr<sub>2</sub>O<sub>3</sub>–Al<sub>2</sub>O<sub>3</sub>–B<sub>2</sub>O<sub>3</sub>- phosphate glasses in SOFC environment [J]. *Journal of Materials Science*, 1998, 33: 2499–2507.
- [17] NIELSEN K A, SOLVANG M, NIELSEN S B L, DINESEN A R, BEEAFF D, LARSEN P H. Glass composite seals for SOFC application [J]. *Journal of the European Ceramic Society*, 2007, 27: 1817–1822.
- [18] BROCHU M, GAUNTT B D, SHAH R, MIYAKE G, LOEHMAN R E. Comparison between barium and strontium-glass composites for sealing SOFCs [J]. *Journal of the European Ceramic Society*, 2006, 26: 3307–3313.
- [19] MAHAPATRA M K, LU K. Seal glass for solid oxide fuel cells [J]. *Journal of Power Sources*, 2010, 195: 7129–7139.
- [20] ATOR D E. Robust copper braze for hermetic sealing of solid oxide fuel cells [D]. Bozeman, Montana: Montana State University, 2008, 90.
- [21] LESSING P A. A review of sealing technologies applicable to solid oxide electrolysis cells [J]. *Journal of Materials Science*, 2007, 42: 3465–3476.
- [22] SINGH R N. Sealing technology for solid oxide fuel cells (SOFC) [J]. *International Journal of Applied Ceramic Technology*, 2007, 4(2): 134–144.
- [23] MALZBENDER J, MONCH J, STEINBRECH R W, KOPPITZ Th, GROSS S M, REMMEL J. Symmetric shear test of glass-ceramic sealants at SOFC operation temperature [J]. *Journal of Materials Science*, 2007, 42: 6297–6301.
- [24] LUO L, LIN Y, HUANG Z, WU Y, SUN L, CHENG L, SHI J. Application of BaO–CaO–Al<sub>2</sub>O<sub>3</sub>–B<sub>2</sub>O<sub>3</sub>–SiO<sub>2</sub> glass–ceramic seals in large size planar IT-SOFC [J]. *Ceramics International*, 2015, 41: 9239–9243.
- [25] HEYDARI F, MAGHSOUDIPOUR A, HAMNABARD Z, FARHANGDOUST S. Evaluation on properties of CaO–BaO–B<sub>2</sub>O<sub>3</sub>–Al<sub>2</sub>O<sub>3</sub>–SiO<sub>2</sub> glass-ceramic sealants for intermediate temperature solid oxide fuel cells [J]. *Journal of Materials Science and Technology*, 2013, 29(1): 49–54.
- [26] HSIANG H I, YUNG S W, WANG C C. Crystallization, densification and dielectric properties of CaO–MgO–Al<sub>2</sub>O<sub>3</sub>–SiO<sub>2</sub> glass with ZrO<sub>2</sub> as nucleating agent [J]. *Materials Research Bulletin*, 2014, 60: 730–737.
- [27] HSIANG H I, YUNG S W, WANG C C. Effects of the addition of alumina on the crystallization, densification and dielectric properties of CaO–MgO–Al<sub>2</sub>O<sub>3</sub>–SiO<sub>2</sub> glass in the presence of ZrO<sub>2</sub> [J].



- Ceramics International, 2014, 40: 15807–15813.
- [28] HEYDARI F, MAGHSOUDIPOURA A, OSTAD SH M, HAMNABARDB Z, FARHANGDOUSTA S [J]. Journal of Ceramic Processing Research, 2014, 15(1): 35–43.
- [29] PARTYKA J. Effect of BaO ratio on the structure of glass–ceramic composite materials from the  $\text{SiO}_2\text{--Al}_2\text{O}_3\text{--Na}_2\text{O--K}_2\text{O--CaO}$  system [J]. Ceramics International, 2015, 41: 9337–9343.
- [30] PARTYKA J. Effect of BaO addition on the structure and microstructure of  $\text{SiO}_2\text{--Al}_2\text{O}_3\text{--Na}_2\text{O--K}_2\text{O--MgO}$  glass-ceramic composites [J]. Ceramics International, 2015, 41: 14013–14020.
- [31] REN X Z, ZHANG W, ZHANG Y, ZHANG P X, LIU J H. Effects of  $\text{Fe}_2\text{O}_3$  content on microstructure and mechanical properties of  $\text{CaO--Al}_2\text{O}_3\text{--SiO}_2$  system [J]. Transactions of Nonferrous Metals Society of China, 2015, 25: 137–145.
- [32] YU Q C, YAN C P, DENG Y, FENG Y B, LIU D C, YANG B. Effect of  $\text{Fe}_2\text{O}_3$  on non-isothermal crystallization of  $\text{CaO--MgO--Al}_2\text{O}_3\text{--SiO}_2$  glass [J]. Transactions of Nonferrous Metals Society of China, 2015, 25: 2279–2284.
- [33] CHEN S, LIN J, YANG H, TANG D, ZHANG T. Controlling the redox reaction at the interface between sealing glasses and Cr-containing interconnect: Effect of competitive reaction [J]. Journal of Power Sources, 2014, 267: 753–759.
- [34] BEST S P, CLARK R J H, HAYWARD C L, WITHNALL R. Polarized single-crystal raman-spectroscopy of danburite,  $\text{CaB}_2\text{Si}_2\text{O}_8$  [J]. Journal of Raman Spectroscopy, 1994, 25: 557–563.
- [35] McKEOWN D A, MULLER I S, BUECHELE A C, PEGG I L, KENDZIORA C A. Structural characterization of-high-zirconia borosilicate glasses using Raman spectroscopy [J]. Journal of Non-Crystalline Solids, 2000, 262: 126–134.
- [36] MAHAPATRA M K, LU K, BODNAR R J. Network structure and thermal property of a novel high temperatures seal glass [J]. Journal of Applied Physics A, 2009, 95: 493–500.
- [37] LU K, MAHAPATRA M K. Network structure and thermal stability study of high temperature seal glass [J]. Journal of Applied Physics, 2008, 104: 074910–074919.
- [38] LENOIR M, GRANDJEAN A, POISSONNET S, NEUVILLE D R. Quantitation of sulfate solubility in borosilicate glasses using Raman spectroscopy [J]. Journal of Non-Crystalline Solids, 2009, 355: 1468–1473.
- [39] GILLET P, DANIEL I, GUYOT F, MATAS J, CHERVIN J C. A thermodynamic model for  $\text{MgSiO}_3$ -perovskite derived from pressure, temperature and volume dependence of the Raman mode frequencies [J]. Physics of the Earth and Planetary Interiors, 2000, 117: 361–384.
- [40] LIU L G, MERNAGH T P, IRIFLJNE T. High pressure Raman spectra of  $\beta\text{-Mg}_2\text{SiO}_4$ ,  $\gamma\text{-Mg}_2\text{SiO}_4$ ,  $\text{MgSiO}_3$ -ilmenite and  $\text{MgSiO}_3$ - perovskite [J]. Journal of Physics and Chemistry of Solids, 1994, 55(2): 185–193.
- [41] CHENG Zh, LIU M. Characterization of sulfur poisoning of Ni-YSZ anodes for solid oxide fuel cells using in situ Raman microspectroscopy [J]. Solid State Ionics, 2007, 178: 925–935.
- [42] LI C, LI M. UV Raman spectroscopic study on the phase transformation of  $\text{ZrO}_2$ ,  $\text{Y}_2\text{O}_3\text{--ZrO}_2$  and  $\text{SO}_4^{2-}/\text{ZrO}_2$  [J]. Journal of Raman Spectroscopy, 2002, 33: 301–308.
- [43] LIU D W, PERRY C H, INGEL R P. Infrared spectra in nonstoichiometric yttria-stabilized zirconia mixed crystals at elevated temperatures [J]. Journal of Applied Physics, 1988, 64: 1413–1417.
- [44] MOON J, CHOI H, KIM Y, LEE C. Cooling rate effect on phase transformation of plasma sprayed partially stabilized zirconia [J]. Journal of Materials Science Letters, 2001, 20: 1611–1613.
- [45] SEKULIC A, FURIC K, TONEJC A, TONEJC A M, STUBICAR M. Determination of the monoclinic, tetragonal and cubic phases in mechanically alloyed  $\text{ZrO}_2\text{--Y}_2\text{O}_3$  and  $\text{ZrO}_2\text{--CoO}$  powder mixtures by Raman spectroscopy [J]. Journal of Materials Science Letters, 1997, 16: 260–262.
- [46] VEIKO V P, BARANOV A V, BOGDANOV K V, FEDOROV A V, YARCHUK M V, IVANOV A I, BERWICK K. Laser-induced thermo-oxidation of thin chromium films: Micro-Raman characterization [J]. Journal of Raman Spectroscopy, 2011, 42(9): 1780–1783.

## 固体氧化物电化学装置用高温 $\text{SiO}_2\text{--Al}_2\text{O}_3\text{--BaO--MgO}$ 和 $\text{SiO}_2\text{--Al}_2\text{O}_3\text{--ZrO}_2\text{--CaO--Na}_2\text{O}$ 玻璃陶瓷密封剂

S. QI<sup>1</sup>, N. M. POROTNIKOVA<sup>2,3</sup>, M. V. ANANYEV<sup>2,3</sup>, A. V. KUZMIN<sup>2,3</sup>, V. A. EREMIN<sup>2,3</sup>, A. A. PANKRATOV<sup>2</sup>, N. G. MOLCHANOVA<sup>2</sup>, O. G. REZNITSKIKH<sup>2</sup>, A. S. FARLENKOV<sup>2,3</sup>, E. G. VOVKOTRUB<sup>2</sup>, Yu. P. ZAIKOV<sup>2,3</sup>

1. 北京化工大学 材料科学与工程学院, 北京 100029;

2. Institute of High-Temperature Electrochemistry of UB RAS, Ekaterinburg 620137, Russia;

3. Ural Federal University named after the First President of Russia B. N. Yeltsin, Ekaterinburg 620002, Russia

**摘要:** 制备了在燃料电池中作为密封剂使用的操作温度可达 700~900 °C 的  $\text{SiO}_2\text{--Al}_2\text{O}_3\text{--BaO--MgO}$  和  $\text{SiO}_2\text{--Al}_2\text{O}_3\text{--ZrO}_2\text{--CaO--Na}_2\text{O}$  系玻璃陶瓷。采用同步热分析和高温膨胀测量技术, 对所研究的玻璃陶瓷的热性能 and 其与燃料电池用材料(YSZ 电解质, 合金连接器 Crofer22APU, 15X25T)的匹配性能进行研究。采用原子发射光谱对玻璃陶瓷的元素成分进行分析。结果表明, 45% $\text{SiO}_2\text{--}15\%\text{Al}_2\text{O}_3\text{--}25\%\text{BaO--}15\%\text{MgO}$  陶瓷的线膨胀系数为  $10.0 \times 10^{-6} \text{ }^\circ\text{C}^{-1}$ , 60% $\text{SiO}_2\text{--}10\%\text{Al}_2\text{O}_3\text{--}10\%\text{ZrO}_2\text{--}5\%\text{CaO--}15\%\text{Na}_2\text{O}$  的为  $9.5 \times 10^{-6} \text{ }^\circ\text{C}^{-1}$ 。采用扫描电镜对 YSZ/玻璃陶瓷/Crofer22APU 的界面结构进行分析。 $\text{SiO}_2\text{--Al}_2\text{O}_3\text{--BaO--MgO}$  玻璃中的硅酸盐相发生了晶化, 采用拉曼光谱和 X 射线衍射对晶化产物进行了分析。与非晶玻璃相比, 所研究的玻璃陶瓷作为电化学或氧传感器中的密封剂使用时具有更佳的性能指标。而  $\text{SiO}_2\text{--Al}_2\text{O}_3\text{--ZrO}_2\text{--CaO--Na}_2\text{O}$  低温非晶陶瓷可以作为燃料电池中的密封剂使用。

**关键词:** 玻璃陶瓷密封剂; 燃料电池; YSZ; Crofer22APU; 硅酸镁

(Edited by Sai-qian YUAN)